The Versatile Transceiver Proof of Concept

J. Troska, S.Detraz, S.Papadopoulos, I. Papakonstantinou, S. Rui Silva, S. Seif el Nasr, C. Sigaud, P. Stejskal, C. Soos, F.Vasey

CERN, 1211 Geneva 23, Switzerland

jan.troska@cern.ch

Abstract

SLHC experiment upgrades will make substantial use of optical links to enable high-speed data readout and control. The Versatile Link project will develop and assess optical link architectures and components suitable for deployment at SLHC. The on-detector element will be bidirectional opto-electronic module: the Versatile Transceiver that will be based on a commercially available module type minimally customized to meet the constraints of the SLHC on-detector environment in terms of mass, volume, power consumption, operational temperature and radiation environment. We report on the first proof of concept phase of the development, showing the steps towards customization and first results of the radiation resistance of candidate optoelectronic components.

I. Introduction

The Versatile Link project [1] aims to provide a multi-gigabit per second optical physical data transmission layer for the readout and control of Super LHC (SLHC) experiments. Point-to-point bidirectional (P2P) as well as point-to-multipoint (PON) architectures are foreseen to be supported by the systems and components currently being assessed and developed. The P2P implementation and its relationship with the GBT project [2] is shown in Figure 1.

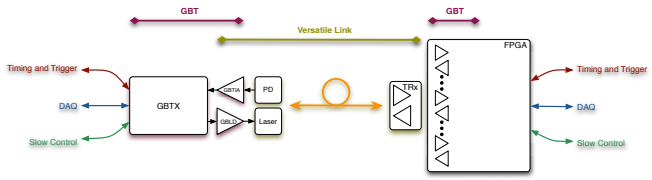

Figure 1: P2P radiation hard optical link for SLHC

The front-end component that will enable the configuration of any of the Versatile Link's supported architectures is a bi-directional module composed of both optical transmitter and receiver: the Versatile Transceiver (VTRx). Both SingleMode (SM) and MultiMode (MM) flavours of the VTRx will be developed to support the various types of installed fibre-plant in the LHC experiments.

Components situated on the detectors at the front-end must meet strict requirements imposed by the operational environment for radiation- and magnetic-field tolerance, low temperature operation (between -40 and -10°C), low mass and volume, and low power consumption. The radiation environment is particularly challenging, as any device placed at the front-end must survive the Si-equivalent of 1.5×10^{15} n (1MeV)/cm^2 fluence and 500kGy ionizing dose. Experience with optical links deployed in LHC experiments has indicated that even the opto-electronic modules situated on the detectors should be sufficiently rugged to allow handling by integration teams relatively unfamiliar with their use. For this reason the VTRx development aims to minimally customize a commercial form factor bidirectional transceiver module that features a direct optical connector interface.

In this paper we will present how we have achieved these goals by providing details of the internals of the module that we have built and showing results of the optoelectronic characterization that has been carried out. Additionally, a critical requirement for the choice of laser- and photo-diodes to be included in the VTRx is that of radiation resistance. A first survey of devices has been carried out to gauge their resistance to displacement damage (the most challenging type of radiation damage for active opto-electronic devices).

II. Packaging

The most promising commercial form factor for modification to meet the needs of operation within the SLHC detectors is the SFP+, which measures approx. 50mm long by 10mm wide by 14mm high. Such a commercial module contains a laser diode driver (LDD) and laser in the transmit path, a photodiode plus transimpedance (TIA) and limiting amplifiers (LA) in the receive path, along with a microcontroller (μC) for module control (Figure 2 a). The VTRx will omit the microcontroller, replace the ASICs with custom-designed radiation resistant versions, and add commercially available laser- and photo-diodes (Figure 2 b) that have been qualified to be sufficiently radiation-resistant.

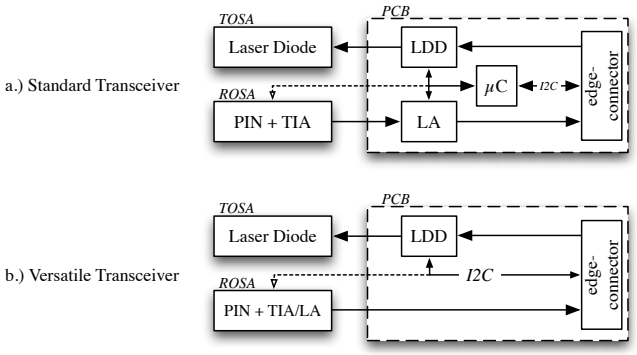

Figure 2: Block diagram of (a) Standard SFP+ transceiver and (b) Versatile transceiver showing the differences between the two.

Work on packaging has been carried out on two major fronts: the investigation of suitable components for inclusion in the VTRX (custom and commercial laser drivers and TIAs,

ROSAs and TOSAs); and becoming familiar with the design issues associated with transceiver packaging through the evaluation of commercial test boards and transceiver modules sourced from an industrial partner as well as the in-house design of test PCBs to evaluate the high-speed components.

We have also successfully tested modified lower-mass SFP+ modules sourced from a commercial transceiver manufacturer. These show that removing material from the metallic SFP+ housing does not adversely affect the performance of individual modules (see Section III for detailed results).

Finally, a study has been carried out to characterize laser diodes through the development of a package and device model that can be used by both ASIC and PCB designers to aid the matching to particular devices. This model [3], with the parameters extracted from the measurement of several candidate laser transmitters, has been successfully used to simulate the performance of a matching network and PCB layout for connection of a laser transmitter to a commercial laser driver. The GBLD [4] designer has also recently used this model to confirm the measured performance of his ASIC.

III. Functional Testing

Two main methods for assessing the functionality of optical transceivers have been adopted: measurement of signal 'eye' diagrams and Bit Error Rate (BER) testing. Both measurement methods have been implemented in our laboratory are used routinely to characterize the performance of components and full transceivers. They are described in detail in Reference [5] and outlined below for completeness.

Measurement of the optical output of a transmitter driven with a pseudorandom bit pattern using a sampling oscilloscope yields an optical eye diagram from which the salient characteristics can be extracted. When such an optical signal is fed back to the optical receiver the same method can be applied to the electrical output of the receiver. Attenuating the optical input to the receiver allows measurement of receiver performance under stressed conditions. We extract metrics such as amplitude, rise/fall times, noise and jitter from such eye diagrams. Figure 3 shows a typical test setup and a typical eye diagram with parameter definitions is shown in Figure 4.

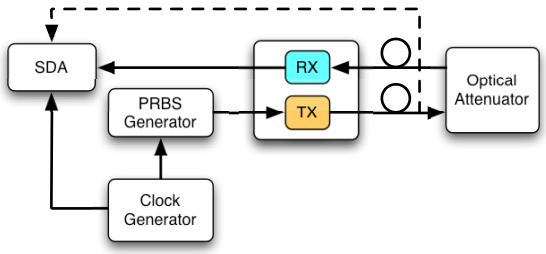

Figure 3: Showing the test setup for eye diagram measurements.

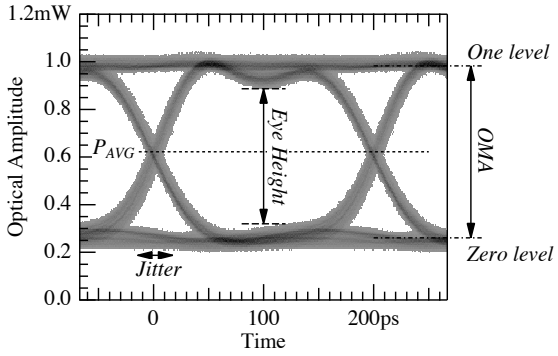

Figure 4: showing a typical eye diagram with parameter definitions.

Measurement of BER as a function of optical modulation amplitude at the receiver allows determination of the receiver sensitivity and thus the overall system power budget. We have implemented a custom BER tester based upon a Xilinx Virtex 5 FPGA evaluation platform that allows us to test not only the basic BER but also the performance of the proposed Forward Error Correction (FEC) code of the GBT protocol [6]. Figure 5 shows a typical test setup.

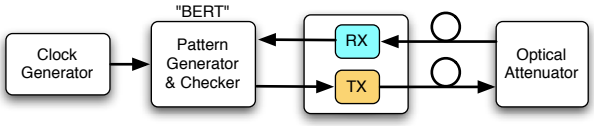

Figure 5: showing the test setup for Bit Error Rate measurements.

We have implemented a visual method for inter-device comparison of the relatively large number of parameters produced per DUT in preparation for being able to compare the relative performance of different components and transceivers. This method creates a so-called Spider- or Radar plot where each parameter is plotted on its own axis and then joining the plotted points on different axes to provide a sort of fingerprint for each DUT that is easily compared visually to the others. An example Spider plot is shown in Figure 6, which shows a comparison of the overall performance of SM and MM transceivers.

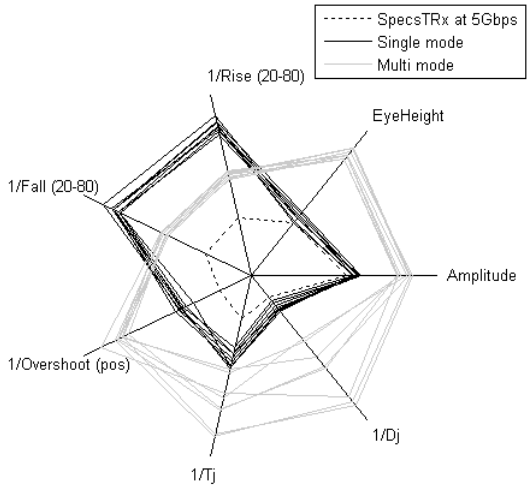

Figure 6: showing an example Spider- or Radar plot comparing the performance of several SM and MM transceiver modules operating at 5Gb/s. Tj and Dj are Total and Deterministic Jitter, respectively.

The Spider plots allow an easy visual comparison between different DUTs, which makes it rather appropriate for investigations involving changes in the transceiver packaging. Figure 7 shows the comparison of three tested generations of SM VTRx prototype: a first standard fully metallic package containing a SM VCSEL transmitter operating at 1310nm; a second standard package containing a DFB edge-emitter; and a third containing the same active components as the second but with a significant amount of metallic shielding removed from the package. Clearly the change in transmitting laser has a large impact on several performance parameters, whereas it is very encouraging that reducing the amount of material appears to have little impact on device performance. We had been concerned that removing material would lead to cross-talk between transmitting- and receiving sides of the VTRx once the electrical shielding was removed, but this appears not to be the case. This result is confirmed by the measurements of MM VTRx prototypes shown in Figure 8, where generation 2 and 3 differ in the packaging only as described for the SM modules.

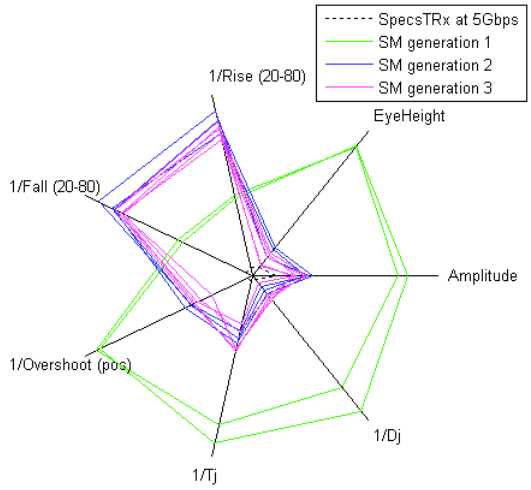

Figure 7: Performance comparison of different SM packaging generations. Values further from the Centre are better.

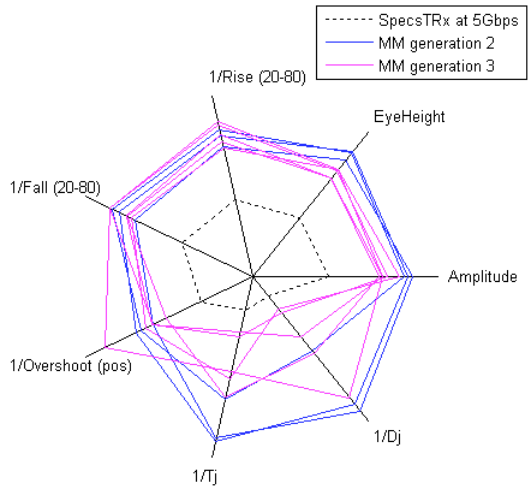

Figure 8: Performance comparison of different MM packaging generations. Values further from the Centre are better.

IV. Radiation Testing

Two radiation tests have been carried out during the first phase of the VTRx development: a Single Event Upset (SEU) test using 60MeV protons at PSI, Villigen, CH and a total fluence test using 20MeV neutrons at the cyclotron facility of UCL, Louvain-la-Neuve, B. The goal of both tests was to survey a large number of devices from different manufacturers in order to compare their relative radiation resistance.

A. SEU Test

The SEU test surveyed SM and MM bare PiN photodiodes and ROSAs by operating them in the proton beam and measuring the effect of the beam on their BER curves. This showed that the passage of particles through the devices can corrupt the data leading to an increase of BER as expected. For operation in SLHC Trackers this increase is beyond tolerable and thus requires the use of FEC in order to guarantee a BER below 10^{-12}. In addition, this test showed that burst errors lasting up to ten consecutive bits can occur in photodiodes, while such bursts may last for hundreds of bits in the case of ROSAs where the receiver TIA is also in the beam. The currently proposed GBT FEC scheme can correct the former but not the latter bursts and so to maintain the BER below 10^{-12} the GBTIA will have to be SEU-hardened by design. Full results have been published [7].

B. Total Fluence Test

The total fluence test surveyed a wide spectrum of commercially available lasers and photodiodes. We have tested single-channel devices from ten different manufacturers. A total of 20 laser devices included two types of 850nm VCSEL, four types of 1310nm Fabry-Perot (FP) edge-emitting laser and three variants of long wavelength (1310/1330/1550 nm) VCSEL. A total of 28 PIN devices included three types of MM GaAs devices and four types of SM InGaAs devices.

The irradiation took place at the cyclotron facility of the Université Catholique de Louvain-la-Neuve in Belgium. Devices were mounted in groups on PCBs that were stacked in front of the neutron-producing Beryllium target. The distance from the target to the devices varied from 13 cm to 18 cm depending upon the location in the stack. Figure 9 shows the fluences reached by the DUTs during the test. There were two periods with no beam due to problems with the operation of the cyclotron.

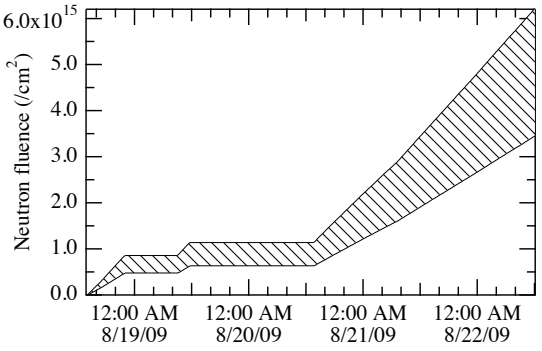

Figure 9: The shaded area represents the range of fluences to which the DUTs were exposed. This variation is due to the distance of individual DUTs from the Beryllium target.

DC device characteristics were measured every twenty minutes during both irradiation and recovery periods. For laser devices we measured their L-I-V curves in order to extract the maximum output power, threshold current, efficiency and series resistance. The progression of the LIV curves during irradiation is shown in Figure 10. For the photodiodes we measured their response to varying levels of light input that allowed us to extract their responsivity and leakage current as a function of applied reverse bias. The typical response for an InGaAs device is shown in Figure 11.

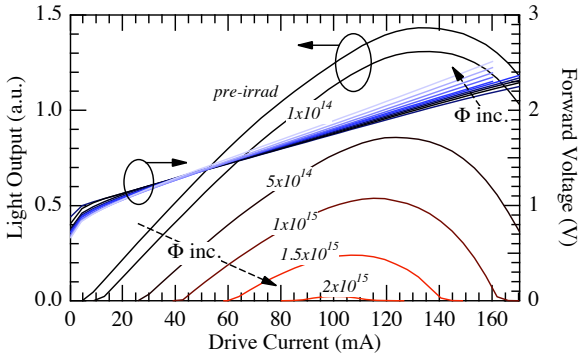

Figure 10: showing the typical behaviour of a laser L-I-V curve during irradiation. The device is a 1310nm FP laser, which stops lasing after a little more than $2x10^{15}$ n/cm^2.

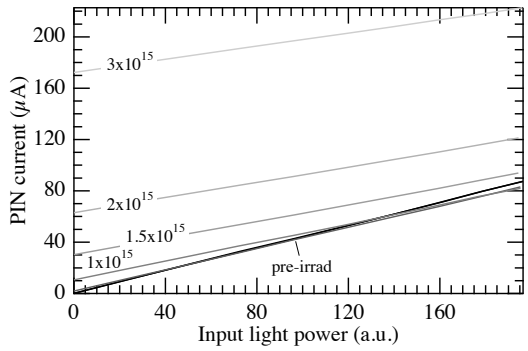

Figure 11: Typical measurement result for a SM PIN showing its response to varying input light power for various increasing levels of irradiation.

For lasers, we show the reduction of the maximum output optical power as a function of total fluence in Figure 12. The smallest active volume devices (MM VCSELs operating at 850nm) showed the highest resistance to radiation damage and remained functional after exposure. All of the longer wavelength SM devices stopped lasing at the highest fluences reached during the test. Of the SM devices again the smaller active volume devices (VCSELs and Quantum Dot lasers) survived to higher fluences than standard edge emitting FP devices. All devices showed recovery after irradiation indicating that the lower flux exposure of the SLHC application will yield less overall damage. Given the observed increases in forward voltage and the already higher pre-irradiation values of the MM VCSELs, further analysis will be required in order to get the full picture of the system implications of these results. Only once this is done can the final conclusion and device selection be carried out.

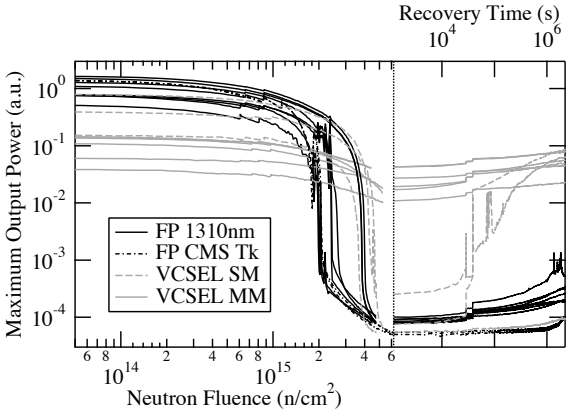

Figure 12: Laser maximum output power as a function of total fluence during irradiation (left-hand side) and then as a function of recovery time (right-hand side).

All InGaAs-based long wavelength devices showed a similar decrease in responsivity (Figure 13) and increase in leakage current (Figure 14), while the GaAs-based devices showed a larger relative drop in responsivity yet no measurable increase in leakage current. The damage in both material types did not anneal post-irradiation. From a system perspective, the lack of leakage current increase in the MM GaAs devices seems very attractive. However, these devices showed a larger relative drop in responsivity and already have a pre-irradiation responsivity value that is at least 50% lower than their SM InGaAs counterparts. So in terms of system margin the final comparison will depend upon the relative impact of increased leakage current on the receiver sensitivity, a parameter that depends entirely on the performance of the transimpedance amplifier (TIA).

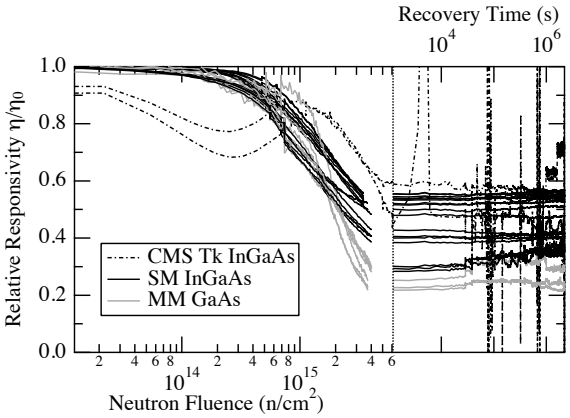

Figure 13: Showing the evolution of PIN responsivity at 2V reverse bias as a function of fluence (left-hand side) and then recovery time (right-hand side).

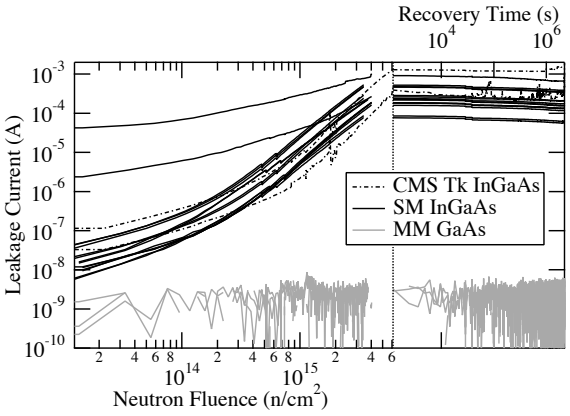

Figure 14: Showing the evolution of PIN leakage current at 2V reverse bias as a function of fluence (left-hand side) and then recovery time (right-hand side).

The data obtained from the total fluence test for lasers are still being analysed to assess whether a shorter irradiation could be used to predict the final outcome, something that is desirable in terms of reducing the cost of future tests.

V. Conclusion

The first phase of development of the VTRx – the front-end component of the Versatile Link – has been successfully completed. We have demonstrated the concept of minimally modifying a commercial transceiver module for use in upgraded SLHC detector systems having removed a significant amount of material and measured no impact on device performance. We have carried out a survey of radiation response to SLHC fluences of a number of commercially available optoelectronic transmitters and receivers. The survey results indicate that we will be able to find a number of commercial devices that are sufficiently radiation resistant to employ in both SM and MM variants of the VTRx.

In the next phase of the project we will further investigate the radiation tolerance of the VTRx and its sub-components. We plan further SEU, total dose and total fluence tests to investigate the details of the radiation response of the components in order to be able to predict the performance of the VTRx once installed in upgraded SLHC detectors.

Further modifications to the VTRx packaging are envisaged in order to reduce the module mass to a strict minimum while ensuring the specified performance of both the VTRx and other parts of the detector systems in which it will be used. The Electromagnetic Compatibility (EMC) properties of the VTRx – that is how much it affects and is affected by its electromagnetic environment – are of particular concern, as the device will be switching relatively large currents at high speeds in the vicinity of the sensitive amplifiers of the detector front-ends.

VI. References

[1] "The Versatile Link, A Common Project For Super-LHC", F. Vasey et al., submitted to JINST

[2] "The GBT Project", P. Moreira et al., these proceedings

[3] "Characterization of Semiconductor Lasers for Radiation Hard High Speed Transceivers", S. Silva et al., these Proceedings

[4] "A 5 Gb/s Radiation Tolerant Laser Driver in 0.13 um CMOS technology", G. Mazza et al., these proceedings

[5] "Evaluation of Multi-Gbps Optical Transceivers for Use in Future HEP Experiments", L. Amaral et al., Proceedings of TWEPP 2008, CERN-2008-008, pp. 151-155

[6] "FPGA-based Bit-Error-Ratio Tester for SEU-hardened Optical Links" C. Soos et al., these proceedings

[7] "Single-Event Upsets in Photoreceivers for Multi-Gb/s Data Transmission", A. Jimenez Pacheco, J. Troska et al., IEEE Trans. Nucl. Sci., Vol. 56, Iss. 4, Pt. 2 (2009), pp. 1978 - 1986